JOURNAL OF INFORMATION SCIENCE AND ENGINEERING 27, 1761-1775 (2011)

Short Paper

Medical Image Registration Based on SVD and Modified PSNR*

MEI-SEN PAN[1,2], JING-TIAN TANG[1] AND XIAO-LI YANG[1]
[1]*Institute of Biomedical Engineering*
Central South University
Changsha, 410083 P.R. China
[2]*College of Computer Science and Technology*
Hunan University of Arts and Science
Changde, 415000 P.R. China

Medical image registration plays a crucial role in clinical diagnosis, treatment, quality assurance, evaluation of curative efficacy and so on. In this paper, by computing the medical image moments, the centroid is obtained, and according to the rotational invariance of the singular values of the matrix of the medical image coordinates, the rotation angles of the reference and floating images are computed respectively, on the foundation of which the initial values for registering the images are generated. When searching the optimal geometric transformation parameters, the modified peak signal-to-noise ratio (*MPSNR*) is selected as the similarity measure, and the simplex method as multi-parameter optimization. The experimental results show that, this proposed method has a fairly simple implementation, a low computational load, a fast registration and good registration accuracy. It also can effectively avoid trapping in the local optimum. Also, the improved iterative closest point algorithm is introduced. The results reveal that the measure deriving the initial values for registration from SVD is potent strategy.

Keywords: singular value decomposition, modified PSNR, medical image, image registration, pixel

1. INTRODUCTION

Medical image registration, as a significant image processing technology, is the operation that applying the spatial geometric transformation to match two or more images acquired from a different time, from a different scene or from a different modality, enables the pixels (voxels) representing the same structure to achieve the space correspondence [1-3]. Over the past several decades, medical image registration technologies have made considerable and dizzying progress, and researchers around the world have presented many ingenious and practical methods, which are basically divided into two broad categories: feature-based and intensity-based medical image registration methods [4]. For

Received December 7, 2009; revised June 22 & November 24, 2010 & February 18, 2011; accepted February 22, 2011.
Communicated by Pau-Choo Chung.
* This paper was partially supported by the Foundation of 11th Five-Year Plan for Key Construction Academic Subject (Optics) of Hunan Province, PRC and supported by Outstanding Young Scientific Research Fund of Hunan Provincial Education Department, PRC (No. 09B071).

the feature-based medical image registration methods, by searching the common, obvious and significant features between the registering images, it obtains the optimal transformation parameters. Among the feature-based registration methods, the iterative closest point (ICP) algorithm pioneered by Besl and Mckay [5] in 1992, is one well known approach and extensively used for the registration on point sets. It can register the point sets without any prior and explicit segmentation or other preprocessing of object features, which makes it be prevalent and very well adapted to point set registration. In the past twenty years, the ICP algorithm has made significant progress, and has further been complemented and perfected. Chen and Medioni [6] and Bergevin *et al.* [7] proposed a precise registration method that finds the closest points based on point-to-plane distances. Rusinkiewicz and Levoy [8] introduced a fast registration method that searches the closet points using point-to-projection metric. Park and Subbarao [9] developed a registration approach that explores the closest points based on contractive-projection-point metric. Although the ICP algorithm is widely used for image registration, it has the following three key problems: (1) It has heavy computational load in the process of searching the corresponding closest points; (2) Whether it successfully gets the optimal registration para- meters strongly depends on the initial rotation and translation matrixes selected. If they are ill-suited, then the registration process needs more searching time, easily gets into the local optima, and even fails to register images; and (3) It is very difficult to automatically acquire the key feature points in image registration.

With respect to the intensity-based image registration, it needn't capture the feature points and only uses the gray level similarity between two images as the registration measure. Because of making full use of image gray information, it has fairly higher registration accuracy. Among intensity-based methods published, the mutual information (*MI*) technology has become one of the most popular methods because it is more flexible and accurate than any other methods in the global information context [4, 10]. In the process of registering the images, it adopts *MI* as similarity measure, and can automatically, directly and accurately register two or more images without any prior segmentation or other preprocessing, which makes it be prevalent and very well adapted to clinical applications. In the literature [11], an alignment method maximizing mutual information of medical images was proposed to obtain the parameters for the translation and rotation needed to register by Paul *et al.* Since the mutual information function contains many local maxima, it easily gets into the local optimum. Therefore, the transformation parameters are not the global optimum ones. The *MI* technology, however, has the following inherent limitations. First, due to the fact that it only considers the gray information instead of or regardless of spatial information, it often traps in the local optimum and even fails to register images. Second, although *MI* reflects the information of the overlapping region between two images, it cannot directly embody the gray discrepancy between two registering images. That is, it cannot be reckoned as the criterion for objectively judging the quality of the registered image. In addition, it has a heavy computational load, time-consuming process and low registration efficiency.

In order to address the above problems, on the basis of a comprehensive and thorough research into the rotational invariance of singular value decomposition (SVD) and peak signal-to-noise ratio (*PSNR*), we propose medical image registration based on SVD and Modified PSNR (*MPSNR*). Also, the method for acquiring the initial values from SVD is adopted for the iterative closest point (ICP) algorithm, and the improved ICP

(IICP) is introduced. The experimental results show that the use of obtaining the initial values by SVD can advance the performance of both *MPSNR* and IICP.

2. DRAWBACKS OF THE MI-BASED IMAGE REGISTRATION

Suppose that reference image $\boldsymbol{R}$ and floating image $\boldsymbol{F}$ are both of $M \times N$ pixels with the upper left pixel being (1, 1) and the gray level being represented by L, and the gray values at point (x, y) are $r(x, y)$ and $f(x, y)$ respectively. The entropy of an image measures the information content contained by the clustering feature of an image gray distribution. For image $\boldsymbol{I}$, its entropy is given by the expression [10],

$$H(\boldsymbol{I}) = -\sum_{k=0}^{L-1} p(k)\log_2 p(k) \tag{1}$$

where $p(k)$ represents the probability function that gray value k appears.

MI, deriving from information theory, is a prevalent entropy-based similarity measure widely used in the medical image field for registration. This measure outperforms most other intensity-based ones in multi-modality registrations because it only assumes a statistical dependence between two images. *MI* is a measure of the degree of dependence of two images. In the process of aligning two or more images, when each point in an image is mapped onto its corresponding point in another image, registration is achieved by maximizing the gray information, that is, the information that an image represents another one is the richest, which is so-called *MI* expressed by:

$$MI(\boldsymbol{R}, \boldsymbol{F}) = H(\boldsymbol{R}) + H(\boldsymbol{F}) - H(\boldsymbol{R}, \boldsymbol{F}) \tag{2}$$

where $H(\boldsymbol{R})$ and $H(\boldsymbol{F})$, are the entropies of reference image $\boldsymbol{R}$ and floating image $\boldsymbol{F}$ respectively, and $H(\boldsymbol{R}, \boldsymbol{F})$ is the joint entropy of $\boldsymbol{R}$ and $\boldsymbol{F}$. In summary, the *MI*-based registration (*MIR*) is described:

$$T_{optimal} = \arg\max_{T} MI(\boldsymbol{R}, T(\boldsymbol{F})). \tag{3}$$

That is, finding an optimal transformation $T_{optimal}$ maximizes the *MI*. Generally, 2-D medical image rigid registration, in essence, includes translation and rotation transformations, namely

$$T = \begin{bmatrix} 1 & 0 & \Delta x \\ 0 & 1 & \Delta y \\ 0 & 0 & 1 \end{bmatrix} \cdot \begin{bmatrix} \cos\phi & -\sin\phi & 0 \\ \sin\phi & \cos\phi & 0 \\ 0 & 0 & 1 \end{bmatrix} \tag{4}$$

where Δx and Δy, express vertical and horizontal displacements respectively, and ϕ denotes the rotation angle. From this, exploring the optimal transformation $T_{optimal}$ is essentially a multi-parameter optimization process as well.

Among the methods of solving the multi-parameter optimization, simplex, pattern

search and Powell methods, as unconstrained optimization ones, are commonly used for registering two images [12]. In the literatures [13, 14], by selecting the *MI* of two registering images as similarity measure, authors adopted Powell, pattern search, and simplex methods to get the translation and rotation transformation parameters. In the process of seeking the optimal solution, these methods have to recursively and iteratively explore the solution space and consequently their computational loads are very heavy. Moreover, whether these optimizing methods successfully get the optimal parameters strongly depends on the initial values selected. If they are ill-suited, then the registration process needs more searching time and even fail to register images.

3. MEDICAL IMAGE REGISTRATION BASED ON SVD AND MODIFIED PSNR

In order to advance registration efficiency and reduce the possibility of failing to register images, this proposed method first acquires the initial values for registering the images to curtail the time for searching the parameter space and to avoid getting into the local optimum, and then selecting *MPSNR* as similarity measure further decreases the time for registering the images.

3.1 Acquisition of the Rotation Angle of the Medical Image

In this paper, suppose that $\boldsymbol{A} \in R^{2\times J}$ with J being a positive integer is a nonsingular matrix, namely, $\boldsymbol{A}$ is a 2-D vector set in the real number space, whose element set is expressed as $[\boldsymbol{X} \quad \boldsymbol{Y}]^T$, where $\boldsymbol{X} = [x_1, x_2, \ldots, x_J]^T$, $\boldsymbol{Y} = [y_1, y_2, \ldots, y_J]^T$.

Theorem 1 Let $\boldsymbol{A} \in R^{2\times J}$, then the singular values of matrix $\boldsymbol{A}$ are invariant to rotation transformation.

Proof: Let matrix $\boldsymbol{A}$ be rotated by the angle ϕ, the rotation matrix is expressed:

$$\boldsymbol{Ro} = \begin{bmatrix} \cos\phi & -\sin\phi \\ \sin\phi & \cos\phi \end{bmatrix},$$

we have

$$\boldsymbol{RoRo}^T = \begin{bmatrix} \cos\phi & -\sin\phi \\ \sin\phi & \cos\phi \end{bmatrix} \cdot \begin{bmatrix} \cos\phi & -\sin\phi \\ \sin\phi & \cos\phi \end{bmatrix}^T = \begin{bmatrix} 1 & 0 \\ 0 & 1 \end{bmatrix}. \tag{5}$$

Then $\boldsymbol{A}_R = \boldsymbol{Ro}^T\boldsymbol{A}$, we get

$$\begin{aligned} \boldsymbol{A}_R^T \boldsymbol{A}_R &= (\boldsymbol{Ro}^T\boldsymbol{A})^T\boldsymbol{Ro}^T\boldsymbol{A} = \boldsymbol{A}^T(\boldsymbol{RoRo}^T)\boldsymbol{A} \\ &= \boldsymbol{A}^T \left(\begin{bmatrix} \cos\phi & -\sin\phi \\ \sin\phi & \cos\phi \end{bmatrix} \cdot \begin{bmatrix} \cos\phi & \sin\phi \\ -\sin\phi & \cos\phi \end{bmatrix} \right) \boldsymbol{A} = \boldsymbol{A}^T\boldsymbol{A}. \end{aligned} \tag{6}$$

$\boldsymbol{A}_R$, therefore, has the same singular values as $\boldsymbol{A}$, that is, the singular values of $\boldsymbol{A}$ is invariant to rotation transformation, which is to be proved.

From the linear algebra perspective, an image is taken as a nonnegative real number matrix. The origin of coordinates is translated to the centroid of the image, $\boldsymbol{P}$ denotes the set of pixel coordinates (x, y) in the translated image, and $J = M \times N$ is the number of elements in $\boldsymbol{P}$. So $\boldsymbol{P} \in R^{2\times J}$ is a 2-D matrix and R is a real number field. According to the definition in the literature [15], there exists a factorization of the form below

$$\boldsymbol{P} = \boldsymbol{U}\boldsymbol{S}\boldsymbol{V}^T \tag{7}$$

where $\boldsymbol{U} \in R^{2\times 2}$ and $\boldsymbol{V} \in R^{J\times J}$ are both orthogonal matrixes, and $\boldsymbol{S} \in R^{2\times J}$ is a diagonal one. Since $\boldsymbol{U} = \begin{bmatrix} U(1, 1) & U(1, 2) \\ U(2, 1) & U(2, 2) \end{bmatrix}$ is unit eigenvectors, for the element $U(1, 2)$ in $\boldsymbol{U}$, the arcsine function is solved and the rotation angle ϕ is obtained according to the description in the literature [5]:

$$\phi = \frac{\arcsin(\boldsymbol{U}(1,\ 2)) * 180}{\pi}. \tag{8}$$

According to the above definitions and theorem, the procedure of getting the rotation angle of the reference image $\boldsymbol{R}$ is shown as follows,

Step 1: The tilt matrix $\boldsymbol{P}_{\boldsymbol{R}} \in R^{2\times(M\times N)}$ is built, which denotes a 2-D matrix of pixel coordinates in the image whose origin of coordinates is translated to the centroid of the reference image $\boldsymbol{R}$

$$\begin{cases} p_{\boldsymbol{R}}(1, (i-1)\times N + j) = (i - \overline{x_{\boldsymbol{R}}}) \times r(i, j) \\ p_{\boldsymbol{R}}(2, (i-1)\times N + j) = (j - \overline{y_{\boldsymbol{R}}}) \times r(i, j) \end{cases} \tag{9}$$

where $i = 1, 2, \ldots, M$, $j = 1, 2, \ldots, N$, $(\overline{x_{\boldsymbol{R}}}, \overline{y_{\boldsymbol{R}}})$ represents the centroid of $\boldsymbol{R}$, and $r(i, j)$ is the gray value at point (i, j) in $\boldsymbol{R}$.

Step 2: According to Eq. (7), by applying SVD to $\boldsymbol{P}_{\boldsymbol{R}}$ $\boldsymbol{U}$ is obtained.

Step 3: According to Eq. (8), the rotation angle $\phi_{\boldsymbol{R}}$ is obtained.

Getting the rotation angle of floating image $\boldsymbol{F}$ has the same process as that of reference image $\boldsymbol{R}$.

3.2 Similarity Measure between Two Images

From the perspective of image restoration, medical image registration is to restore the floating image with geometric distortion to the reference image. Therefore, there must be a criterion to be used for objectively evaluating the quality of the restored image. Although the *MI* well reflects the information of the overlapping region between two images, it cannot directly and globally exemplify the gray difference between the images. At the

Table 1. Computational load of *MI*.

	Operation	$H(\boldsymbol{R})$	$H(\boldsymbol{F})$	$H(\boldsymbol{R}, \boldsymbol{F})$	Total
Solving probability	Addition	MN	MN	MN	$3MN$
	Division	L	L	L^2	$L^2 + 2L$
Solving entropy	Logarithm	L	L	L^2	$L^2 + 2L$
	Multiplication	L	L	L^2	$L^2 + 2L$
	Addition	L	L	L^2	$L^2 + 2L$

same time, it has a heavy computational load and a time-consuming operation. Table 1 shows the computational load of the *MI* between reference image $\boldsymbol{R}$ and floating image $\boldsymbol{F}$, which denotes that the load depends on the image gray level L as well as on the size $M \times N$ of the image. In Table 1, the multiplication, division and logarithm operations only relate to the gray level L, while they are fairly time-consuming.

Since *PSNR* can firsthand and overall represent the distinction between images, so far it is an extensively-used criterion that gauges the quality of a restored image. Generally speaking, the greater the value *PSNR*, the smaller the difference between images, the more similar two images, and the better the quality of the restored image; contrarily, with a smaller value, the difference is greater, two images are more different, and the quality is poorer. *PSNR* is defined as

$$PSNR = 10 \log_{10} \left(\frac{M \times N \times (L-1)^2}{\sum_{x=1}^{M} \sum_{y=1}^{N} (r(x, y) - f(x, y))^2} \right). \tag{10}$$

In order to compare with the computational load of the *MI*, Table 2 expounds the computational load of the *PSNR*. Compared with *MI*, *PSNR* enjoys a better advantage. Therefore, in this paper, we use *PSNR* as the similarity measure between the reference and floating images. Herein Eq. (3) is rewritten

$$T_{optimal} = \arg\max_{T} PSNR(\boldsymbol{R}, T(\boldsymbol{F})). \tag{11}$$

Table 2. Computational load of *PSNR*.

Operation	*PSNR*	Total
Addition	MN	MN
Division	1	1
Logarithm	1	1
Multiplication	MN	MN
Subtraction	MN	MN

That is, searching an optimal transformation $T_{optimal}$ maximizes the value *PSNR* of the registered floating image.

In the actual image registration, generally, $\sum_{x=1}^{M} \sum_{y=1}^{N} (r(x, y) - f(x, y))^2 = 0$ is almost

Fig. 1. Reference image.

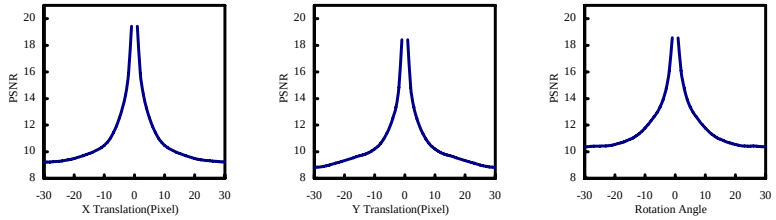

(a) X translation. (b) Y translation. (c) Rotation.

Fig. 2. Change curve of PSNR.

impossible in Eq. (10). However, theoretically, $\sum_{x=1}^{M}\sum_{y=1}^{N}(r(x,y)-f(x,y))^2=0$ is possible in the process of the image self-registration. For instance, Fig. 1 is a reference image. We impose the self-registration on the image in Fig. 1 by applying the X, Y coordinate translations and image rotation, respectively, and the three change curves of *PSNR* are shown in Fig. 2.

As shown in Fig. 2, we can see clearly the breaks in the change curves of *PSNR* at the zero-crossing point of the horizontal axis, which results from $\sum_{x=1}^{M}\sum_{y=1}^{N}(r(x,y)-f(x,y)^2 = 0$ and then $PSNR = \infty$ in the process of the image self-registration. Eq. (10), therefore, must be modified with a complementary value Δd. Then we get the *MPSNR*,

$$MPSNR = 10\log_{10}\left(\frac{M\times N\times(L-1)^2}{\sum_{x=1}^{M}\sum_{y=1}^{N}(r(x,y)-f(x,y))^2+\Delta d}\right). \tag{12}$$

Similarly Eq. (11) is rewritten

$$T_{optimal} = \arg\max_{T} MPSNR(\boldsymbol{R}, T(\boldsymbol{F})). \tag{13}$$

Now we discuss the complementary value Δd. According to Eq. (12), we get

$$\sum_{x=1}^{M}\sum_{y=1}^{N}(r(x,y)-f(x,y))^2+\Delta d=\frac{M\times N\times(L-1)^2}{10^{\frac{MPSNR}{10}}}. \tag{14}$$

For Eq. (14), since

$$\sum_{x=1}^{M}\sum_{y=1}^{N}(r(x,y)-f(x,y))^2 \geq 0,$$

we derive that

$$0 < \Delta d \leq \frac{M \times N \times (L-1)^2}{10^{\frac{MPSNR}{10}}}. \tag{15}$$

On the basis of a lot of experiments, we find that

$$10 \times M \times N \geq 10^{\frac{MPSNR}{10}}. \tag{16}$$

Combining Eqs. (15) and (16) yields

$$\frac{M \times N \times (L-1)^2}{10 \times M \times N} \leq \frac{M \times N \times (L-1)^2}{10^{\frac{MPSNR}{10}}}. \tag{17}$$

We therefore can make

$$\Delta d \leq \frac{M \times N \times (L-1)^2}{10 \times M \times N} = \frac{(L-1)^2}{10}. \tag{18}$$

In this paper, we choose $\Delta d = \frac{(L-1)^2}{10}$ and then Eq. (12) is rewritten

$$MPSNR = 10 \log_{10}\left(\frac{M \times N \times (L-1)^2}{\sum_{x=1}^{M}\sum_{y=1}^{N}(r(x,y)-f(x,y))^2 + \frac{(L-1)^2}{10}}\right). \tag{19}$$

According to Eq. (13), by applying the image self-registration to Fig. 1 the change curves of *MPSNR* are obtained, shown in Fig. 3. According to the Fig. 3, due to the presence of the complementary value Δd, there exist no breaks in the change curves of MPSNR and each curve is smooth and continuous. In addition, we also perform the image self-registration to Fig. 1 by using *MI* as the similarity measure, and the change curves are shown in Fig. 4. Fig. 5 shows the average computational load of *MI* and *MPSNR*.

In Figs. 3-4, at zero-crossing point, compared with *MI*, *MPSNR* has a much narrower and steeper curve and thus more easily gets accurate registration parameters. From Fig. 5, the average computational load of *MPSNR* is much superior to that of *MI*, which is in accordance with the analysis for Tables 1 and 2 in section 3.2.

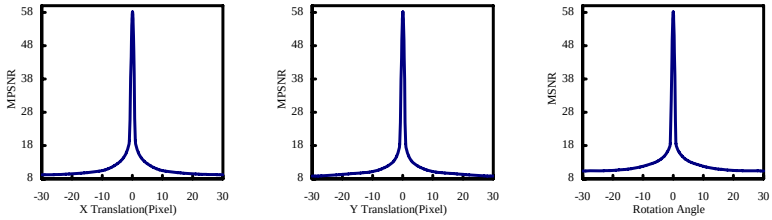

(a) X translation. (b) Y translation. (c) Rotation.

Fig. 3. Change curves of *MPSNR*.

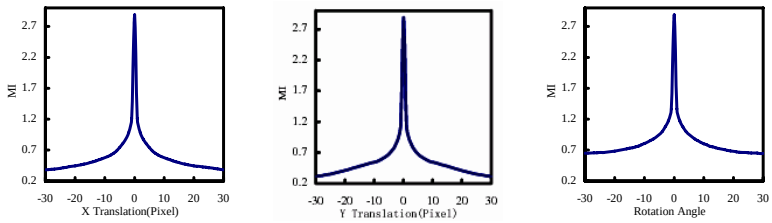

(a) X translation. (b) Y translation. (c) Rotation.

Fig. 4. Change curves of *MI*.

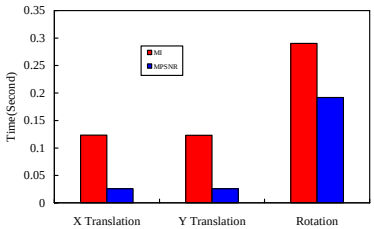

Fig. 5. Average computational load of *MI* and *MPSNR*.

3.3 Procedure of this Proposed Method

As mentioned before, medical image registration based on SVD and *MPSNR* (RSMP) is detailedly depicted as follows,

Step 1: According to the image moments [16], the centroids $(\overline{x_R}, \overline{y_R})$ and $(\overline{x_F}, \overline{y_F})$ of reference image $\boldsymbol{R}$ and the floating image $\boldsymbol{F}$, are computed respectively.

Step 2: According to the rotational invariance of the singular values of the matrix of the medical image coordinates, the rotation angles ϕ_R and ϕ_F of reference image $\boldsymbol{R}$ and floating image $\boldsymbol{F}$, are obtained respectively.

Step 3: The initial values for registering the images are calculated, namely, $\Delta x_0 = \overline{x_F} - \overline{x_R}$, $\Delta y_0 = \overline{y_F} - \overline{y_R}$, $\Delta\phi_0 = \phi_F - \phi_R$.

Step 4: Selecting *MPSNR* as the similarity measure, and the simplex method as a multi-parameter optimizing method, is applied to get the translation and rotation parameters.

Step 5: The optimizing process ends and the optimal transformation $T_{optimal}$ is procured.

4. THE IMPROVED ITERATIVE CLOSEST POINT ALGORITHM

Since the ICP algorithm has some setbacks mentioned above, IICP are proposed in the section. IICP first utilizes image moments and SVD to obtain the centroids and rotation angles of the reference and floating images respectively, and then Canny operator to automatically acquire the feature points. As stated above, IICP is delineated in detail as follows,

Step 1: According to the image moments [16], the centroids $(\overline{x_{\boldsymbol{R}}}, \overline{y_{\boldsymbol{R}}})$ and $(\overline{x_{\boldsymbol{F}}}, \overline{y_{\boldsymbol{F}}})$ of reference image $\boldsymbol{R}$ and the floating image $\boldsymbol{F}$, are computed respectively.

Step 2: According to the rotational invariance of the singular values of the matrix of the medical image coordinates, the rotation angles $\phi_{\boldsymbol{R}}$ and $\phi_{\boldsymbol{F}}$ of reference image $\boldsymbol{R}$ and floating image $\boldsymbol{F}$, are obtained respectively.

Step 3: The initial values for registering the images are calculated, namely, $\Delta x_0 = \overline{x_{\boldsymbol{F}}} - \overline{x_{\boldsymbol{R}}}$, $\Delta y_0 = \overline{y_{\boldsymbol{F}}} - \overline{y_{\boldsymbol{R}}}$, $\Delta\phi_0 = \phi_{\boldsymbol{F}} - \phi_{\boldsymbol{R}}$.

Step 4: Δx_0, Δy_0 and $\Delta\phi_0$ are used as the initial translation and rotation parameters for the ICP algorithm, namely

$$R_0 = \begin{bmatrix} \cos(\Delta\phi_0) & -\sin(\Delta\phi_0) \\ \sin(\Delta\phi_0) & \cos(\Delta\phi_0) \end{bmatrix}, \; T_0 = [\Delta x_0 \quad \Delta y_0]^T.$$

Step 5: Canny operator is first imposed on the reference image $\boldsymbol{R}$ and the floating image $\boldsymbol{F}$ respectively, and then binarized images $\boldsymbol{B_R}$ and $\boldsymbol{B_F}$ are generated.

Step 6: Two point sets of coordinates representing all the pixels with gray values being 1 or 255 in the images $\boldsymbol{B_R}$ and $\boldsymbol{B_F}$ respectively, are obtained, and they are selected as the reference and floating point sets in the ICP algorithm.

Step 7: The ICP algorithm is performed and the final rotation matrix R_0 and translation T_0 are derived.

5. EXPERIMENTS AND RESULTS

In this paper, all the experimental slice images are taken from the brain image database built by Retrospective Image Registration Evaluation Projection, which is affiliated to Vanderbilt University, USA. RSMP is implemented in MATLAB 7.1 on PC with a Pentium IV 2.6 GHz and 1024MB RAM, running Windows XP. To compare the accuracy of image registration, we define error ρ_i,

$$\rho_i = \frac{|\Delta i - \Delta i_s|}{|\Delta i_s|} \times 100\% \quad (i = x, y, \phi) \tag{20}$$

where Δi_s is the standard transformation parameter aligning the floating image with the reference image, and Δi represents the actual transformation parameter acquired by the registration method mentioned in this paper. Further, we define total error ρ,

$$\rho = \sum_{i=\{x,y,\phi\}} \rho_i. \tag{21}$$

5.1 Multi-Modality Image Registration Based on *MPSNR* and *MIR*

In the section, we use No. 22 CT, No. 20 MR_T1 and No. 12 PET brain images of the patient_001 as the reference images. The experimental images are divided into the following three groups. The first is to select MR image as the reference one and, CT1 and CT2 as the floating images, whose sizes are of 256 × 256 pixels, shown in Fig. 6. The second is to select MR image as the reference one and, PET1 and PET2 as the floating images, whose sizes are of 128 × 128 pixels, shown in Fig. 7. And the last is to select CT image as the reference one and, PET1 and PET2 as the floating images, whose sizes are of 128 × 128 pixels, shown in Fig. 8. The gray levels of these experimental images above are all represented by 256. In the experiments, RSMP first and then *MIR* are applied to register the multi-modality images respectively, and we use the simplex method to search the optimal registering parameters. The remarked difference from the experiments of the mono-modality image registration, is that the actual space transformation parameters of registering the images are unknown in the multi-modality image registration. So we apply SVD to obtain the initial values for registration. Assume that the initial values are relatively accurate and they are taken as Δi_s in Eq. (20), shown in Table 3.

Δx_0, Δy_0 and ϕ_0 acquired by applying SVD, are used for the initial values of the simplex method, shown in Table 3. The experimental results based on RSMP and *MIR* are shown in Figs. 9-10 and Table 4, respectively.

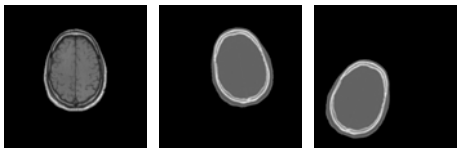

(a) MR. (b) CT1. (c) CT2.

Fig. 6. The first group of images.

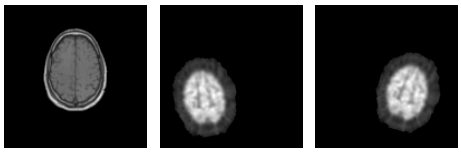

(a) MR. (b) PET1. (c) PET2.

Fig. 7. The second group of images.

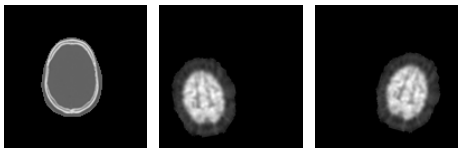

(a) CT. (b) PET1. (c) PET2.

Fig. 8. The third group of images.

Table 3. Transformation parameters of multi-modality float images.

Parameter	Floating image					
	The first group		The second group		The third group	
	CT1	CT2	PET1	PET2	PET1	PET2
Δx_s/Pixel	– 8.465	47.678	22.716	18.023	17.555	12.862
Δy_s/Pixel	19.246	– 47.022	– 24.003	18.891	– 20.748	22.146
$\Delta\phi_s$ (°)	11.687	– 21.285	13.406	– 12.861	14.202	– 12.065

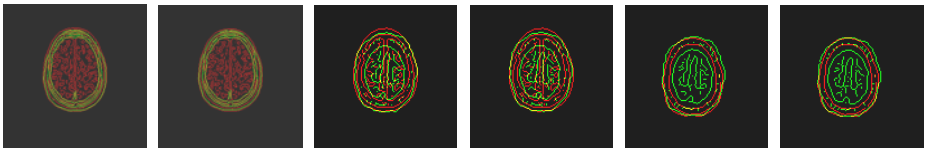

(a) MR&CT1. (b) MR&CT2. (c) MR&PET1. (d) MR&PET2. (e) CT&PET1. (f) CT&PET2.

Fig. 9. Result figures of registering the multi-modality images using RSMP.

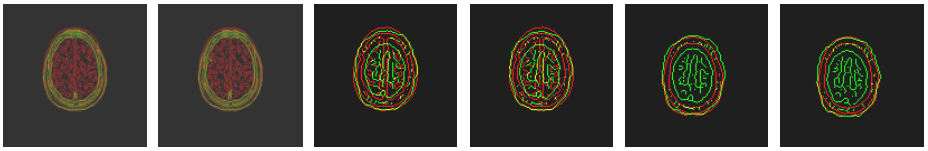

(a) MR&CT1. (b) MR&CT2. (c) MR&PET1. (d) MR&PET2. (e) CT&PET1. (f) CT&PET2.

Fig. 10. Result figures of the multi-modality images using *MIR*.

Table 4. Performance of registering multi-modality images based on RSMP and *MIR*.

Images	Registration method	Parameter				Error			
		Δx	Δy	$\Delta\phi$	Time/S	ρ_x	ρ_y	ρ_ϕ	ρ
MR CT1	RSMP	– 7.6628	20.2732	11.6049	4.672	9.4767	5.3372	0.7025	15.5164
	MIR	– 7.6155	20.334	10.765	6.891	10.0354	5.6531	7.8891	23.5776
MR CT2	RSMP	49.3797	– 50.858	– 20.718	5.36	3.5692	8.1575	2.6629	14.3896
	MIR	48.713	– 50.666	– 20.019	7.562	2.17081	7.7489	5.9488	15.8685
MR PET1	RSMP	21.8326	– 23.561	14.1582	1.532	3.8889	1.8435	5.6109	11.3433
	MIR	22.7923	– 23.155	14.1105	2.562	0.3359	3.5346	5.2551	9.1256
MR PET2	RSMP	17.9995	18.9994	– 13.464	1.109	0.1304	0.5738	4.6901	5.3943
	MIR	18	19	– 13.504	1.968	0.1276	0.5770	4.9973	5.7019
CT PET1	RSMP	17.793	– 21.009	14.5686	1.438	1.3557	1.2570	2.5813	5.1940
	MIR	17.3846	– 21.512	14.0551	2.36	0.9707	3.6813	1.0344	5.6864
CT PET2	RSMP	13.1811	21.9979	– 12.403	1.281	2.4810	0.6687	2.8048	5.9545
	MIR	12.6208	22.6865	– 12.341	1.922	1.8753	2.4406	2.2909	6.6068

According to the registering results from Table 4, the registering speed of RSMP has is considerably superior to that of *MIR*, especially for the larger image. According to Eqs. (20)-(21), we obtain the registration errors of RSMP and *MIR*, listed in Table 4. The experimental results indicate that, the registration accuracy of RSMP, overall, achieves that of *MIR* or even better. Therefore, selecting *MPSNR* as the similarity measure in the multi-modality image registration is the same effective criterion as *MI*.

5.2 Multi-Modality Medical Image Registration Based on ICP and IICP

We still use the experimental images in section 4.1. The ICP algorithm first and then IICP are applied to register the multi-modality medical images, respectively, and the experimental results are shown in Figs. 11-12 and Table 5.

From Table 5, the processing time of IICP is relatively superior to that of the ICP, especially for the larger image. From Figs. 11-12, the ICP algorithm fails to register all

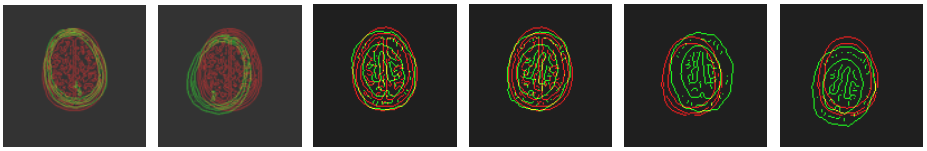

(a) MR&CT1. (b) MR&CT2. (c) MR&PET1. (d) MR&PET2. (e) CT&PET1. (f) CT&PET2.
Fig. 11. Result figures of registering the multi-modality images using the ICP algorithm.

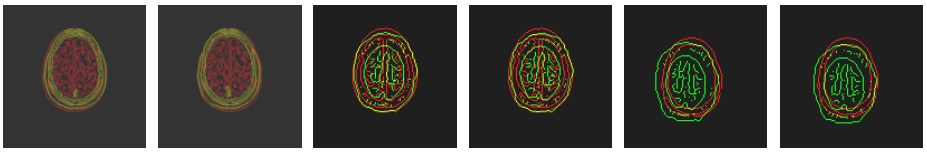

(a) MR&CT1. (b) MR&CT2. (c) MR&PET1. (d) MR&PET2. (e) CT&PET1. (f) CT&PET2.
Fig. 12. Result figures of the multi-modality images using IICP.

Table 5. Performance of registering multi-modality images based on ICP and IICP.

Images	Registration method	Parameter				Error			
		Δx	Δy	$\Delta\phi$	Time/S	ρ_x	ρ_y	ρ_ϕ	ρ
MR CT1	ICP	– 2.7602	18.8546	0.1573	2.388	67.3928	2.03367	98.6541	168.081
	IICP	– 7.4779	19.9363	11.6301	2.25	11.6610	3.58672	0.48687	15.7345
MR CT2	ICP	43.9351	– 30.939	– 5.2235	11.14	7.85037	34.2023	75.4592	117.512
	IICP	52.5442	– 50.479	– 21.280	1.781	10.2064	7.35167	0.02537	17.5834
MR PET1	ICP	22.6715	– 23.425	0.1541	0.956	0.1959	2.40845	98.8505	101.455
	IICP	21.6496	– 23.298	13.4259	0.89	4.69449	2.93588	0.14844	7.7788
MR PET2	ICP	17.1802	20.7187	– 0.4464	1.172	4.67625	9.67498	96.5290	110.880
	IICP	16.6652	17.8058	–12.872	0.953	7.53371	5.74453	0.08242	13.3607
CT PET1	ICP	21.2474	– 29.191	5.7841	3.375	21.0333	40.6931	59.2726	120.999
	IICP	11.9755	– 17.448	11.0438	3.187	31.7830	15.9037	22.2377	69.9244
CT PET2	ICP	4.7543	26.7589	– 4.1211	2.843	63.0361	20.8250	65.8425	149.704
	IICP	8.4037	26.7706	–16.669	0.5798	34.6626	20.8823	38.1600	93.7049

the images, while IICP is successful in registering most of the images, which is in accordance with the errors derived from Table 5. Therefore IICP needs to be further improved in the multi-modality registration. As stated above, the use of SVD is still an effective measure for generating initial values.

5.3 Comparisons of RSMP and IICP

RSMP and IICP, as explained above, due to the use of obtaining the initial values for registration by SVD, their registration accuracy are greatly advanced and their processing time are significantly reduced. In addition, RSMP also benefits from the new, fast similarity measure, and IICP also takes advantage of the automatic feature point extraction by Canny operator. However, RSMP and IICP are still obvious differences in the performance. In the multi-modality image registration, RSMP can successfully register all the images, but IICP only can align most of all the images. With respect to the registra-

tion accuracy, RSMP is more excellent method compared with IICP. Considering the processing time, IICP is superior to RSMP.

6. CONCLUSION

In order to solve the existing problems of registering the images based on *MI* and SVD, by using the rotational invariance of SVD as the tool for getting the image rotation angle, *MPSNR* as the similarity measure between the reference and floating images, and the simplex method as the optimizing means, medical image registration based on SVD and *MPSNR* is presented. The experimental results reveal that, RSMP has a simple logical structure, a short computation, a fast registration and a high accuracy, and also overcomes the problem of easily getting into the local optimum. It can be well suitable for both mono-modality and multi-modality image registrations. In addition, the use of obtaining the initial values by SVD also can help the ICP algorithm to boost the performance. The study of applying RSMP to the non-rigid medical image registration will be the focus of a next research.

REFERENCES

1. Z. T. Lu, Y. Q. Feng, Q. J. Feng, and W. F. Chen, "Medical image registration based on principal phase congruency," *ACTA Electronica Sinica*, Vol. 36, 2008, pp. 1974-1978.
2. J. Kybic and M. Unser, "Fast parametric elastic image registration," *IEEE Transactions on Image Processing*, Vol. 12, 2003, pp. 1427-1442.
3. J. F. Krucker, G. L. LeCarpentier, J. B. Fowlkes, and P. L. Carson, "Rapid elastic image registration for 3-D ultrasound," *IEEE Transactions on Medical Imaging*, Vol. 21, 2002, pp. 1384-1394.
4. J. B. Antoine Maintz and M. A. Viergever, "A survey of medical image registration," *Medical Image Analysis*, Vol. 2, 1998, pp. 1-36.
5. P. J. Besl and N. D. Mckay, "A method for registration of 3-D shapes," *IEEE Transactions on Pattern Analysis and Machine Intelligence*, Vol. 14, 1992, pp. 239-256.
6. Y. Chen and G. Medioni, "Object modeling by registration of multiple range images," *Image and Vision Computing*, Vol. 10, 1992, pp. 145-155.
7. R. Bergevin, M. Soucy, H. Gagnon, and D. Laurendeau, "Towards a general multiview registration technique," *IEEE Transactions on Pattern Analysis and Machine Intelligence*, Vol. 18, 1996, pp. 540-547.
8. S. Rusinkiewicz and M. Levoy, "Efficient variants of the ICP algorithm," in *Proceedings of the 3rd International Conference on 3-D Digital Imaging and Modeling*, 2001, pp. 145-152.
9. S. Y. Park and M. Subbarao, "Automatic 3D model reconstruction based on novel pose estimation and integration techniques," *Image and Vision Computing*, Vol. 22, 2004, pp. 623-635.
10. J. P. W. Pluim, J. B. A. Maintz, and M. A. Viergever, "Mutual-information-based registration of medical images: a survey," *IEEE Transactions on Medical Imaging*, Vol. 22, 2003, pp. 986-1004.

11. V. Paul, M. William, and I. Wells, "Alignment by maximization of mutual information," *International Journal of Computer Vision*, Vol. 24, 1997, pp. 137-154.
12. J. L. Andersson, A. Sundin, and S. Valind, "A method for coregistration of PET and MR brain image," *Journal of Nuclear Medicine*, Vol. 36, 1995, pp. 1307-1315.
13. B. W. Fei, A. Wheaton, Z. Lee, J. L. Duerk, and D. L. Wilson, "Automatic MR volume registration and its evaluation for the pelvis and prostate," *Physics in Medicine and Biology*, Vol. 47, 2002, pp. 823-838.
14. P. J. Slomka, J. Mandel, D. Downey, and A. Fenster, "Evaluation of voxel-based registration of 3-D power doppler ultrasound and 3-D magnetic resonance angiographic images of carotid arteries," *Ultrasound in Medicine and Biology*, Vol. 27, 2001, pp. 945-955.
15. V. Klema and A. Laub, "The singular value decomposition: Its computation and some applications," *IEEE Transactions on Automatic Control*, Vol. 25, 1980, pp. 164-176.
16. M. Hu, "Visual pattern recognition by moment invariants," *IRE Transactions on Information Theory*, Vol. 8, 1962, pp. 179-187.

Mei-Sen Pan (潘梅森) graduated from Hunan Normal University, China, in 1995. He received the M.S. degree from Huazhong University of Science and Technology, China, in 2005. He is currently a Professor in Hunan University of Arts and Science, and also a Ph.D. candidate in Central South University, PRC. He has published more than 25 papers in journals and conferences. His research interests include biomedical image processing, information fusion, artificial neural network and software engineering.

Jing-Tian Tang (汤井田) graduated and received the M.S. degree from Changchun University of Earth Sciences, China, in 1986 and 1988, respectively. He received the Ph.D. degree from Central South University, China, in 1992. He is currently a Professor and Ph.D. supervisor of Central South University, PRC. He has published more than 70 papers in journals and conferences. He research interests include geophysical inverse method and theory, and medical signal processing. He presided over many state-level key projects.

Xiao-Li Yang (杨晓利) graduated from Hunan Medical Specialty High School, China, in 2001. She received the M.S. degree from Central South University of Biomedical Technology, China, in 2008. She is currently a Ph.D. candidate in Central South University, PRC. She has published more than 4 papers in journals and conferences. Her research interests include biomedical image and signal processing.